Hydroxyapatite Reinforced Magnesium Alloy Composites Using the Ultrasonic-Assisted Rheo-Squeeze Casting Technique: Microstructural and Mechanical Performance Evaluation

crystals

MDPI

Article

Hydroxyapatite Reinforced Magnesium Alloy Composites Using the Ultrasonic-Assisted Rheo-Squeeze Casting Technique: Microstructural and Mechanical Performance Evaluation for Bone Fixture Applications

Arunkumar Thirugnanasambandam [1,*], Ashokkumar Mohankumar [1], Rajendra Prasad Reddy Botta [2], William Woei Fong Chong [3], Geethapriyan Thangamani [4] and Manoj Gupta [5,*]

[1] Centre for Sustainable Materials and Surface Metamorphosis, Chennai Institute of Technology, Chennai 600069, India
[2] Department of Mechanical Engineering, CMR Institute of Technology, Bengaluru 560037, India
[3] Automotive Development Centre, Institute for Vehicle Systems and Engineering (IVeSE), Universiti Teknologi Malaysia, Johor Bahru 81310, Malaysia; william@utm.my
[4] Politecnico di Torino, Corso Duca degli Abruzzi 24, 10129 Torino, Italy; devimani.priyan18@gmail.com
[5] Department of Mechanical Engineering, National University of Singapore, 9 Engineering Drive 1, Singapore 117575, Singapore
* Correspondence: arunkumar.t@citchennai.net (A.T.); mpegm@nus.edu.sg (M.G.)

Abstract: Magnesium-based biomaterials have recently been in the research spotlight in the field of biomedical engineering owing to their properties, such as density and biocompatibility that closely align with those of human bone. However, poor strength and rapid degradation impede their application as bone support fixtures. The present research aims to tailor the properties of Mg by using a novel ultrasonic-assisted rheo-squeeze casting approach. To satisfy the demand, pure Mg (Mg), MHA (Mg/5%HA), MZHA (Mg-1%Zn/5%HA/), and MSHA (Mg-1%Sn/5%HA) were fabricated, and various mechanical tests were conducted to assess the composite's mechanical properties, including its microhardness, tensile strength, compressive strength, flexural strength, and impact strength. The microstructural and fractured morphology of the composites was examined by scanning electron microscopy (SEM), whereas their elemental composition was analyzed by field emission scanning electron microscopy (FESEM) equipped with elemental mapping. Comparing the MZHA, MHA, and pure Mg samples, the mechanical behavior of MSHA is significantly superior. This is due to composites containing Sn that possess finer-grained materials, which act as barriers to dislocation motion while increasing the strength of the materials. From the observed results, there is a significant improvement in the microhardness of MSHA of 64.5% when compared to that of pure Mg, and 42.7% compared to MHA. Furthermore, MSHA composites possess noticeable enhancements in tensile and compression performance of 80.8% and 58.3%, respectively, and 19% and 22.4% compared to MHA. Additionally, the impact and flexural performance of MSHA composites exhibit higher performance (41% and 42%) than pure Mg and 8% and 7% against the MHA composite.

Keywords: pure magnesium; composite materials; ultrasonic assisted rheo-squeeze casting; mechanical performance

Citation: Thirugnanasambandam, A.; Mohankumar, A.; Reddy Botta, R.P.; Chong, W.W.F.; Thangamani, G.; Gupta, M. Hydroxyapatite Reinforced Magnesium Alloy Composites Using the Ultrasonic-Assisted Rheo-Squeeze Casting Technique: Microstructural and Mechanical Performance Evaluation for Bone Fixture Applications. *Crystals* **2024**, *14*, 667. https://doi.org/10.3390/cryst14070667

Academic Editor: Marek Sroka

Received: 26 June 2024
Revised: 16 July 2024
Accepted: 18 July 2024
Published: 21 July 2024

1. Introduction

Biocompatibility and biodegradability are two of the unique properties of magnesium alloys that have made them very promising for use in biomedical applications in recent years [1]. Magnesium alloys are in high demand for application in biomedical devices such as orthopedic implants (temporary bone support fixtures) due to their properties that closely resemble those of natural bone [2]. Because of the higher strength over natural

bone, conventional metallic implants, consisting of stainless steel, Ti-based alloys, and cobalt–chromium alloys, generate unbalanced stress concentrations and stress shielding phenomena in the area of implant placement. To circumvent this, magnesium-based materials are being extensively investigated as an alternative to traditional metal implants because of their striking resemblance to real bone [3]. Despite their potential, pure magnesium and its alloys are not extensively employed in biomedical implants due to several issues. However, these materials are weak and break down quickly in a physiological medium, which could compromise the integrity of the implant and necessitate replacements on a recurring basis [4]. Researchers are striving to develop innovative strategies that will enhance the mechanical properties and corrosion resistance of magnesium-based biomaterials while preserving their biocompatibility in order to overcome these challenges and realize the full potential of these materials [5–7]. Alloying, surface treatments, and magnesium-based composite fabrications are various techniques where researchers are trying to improve the suitability of magnesium-based materials for implant applications [8]. From the above-mentioned methods, alloying and composite-making techniques are proven to improve the strength of Mg-based materials. However, the galvanic corrosion tendency might limit their performance when pure Mg is alloyed with other noble metals. Adding bioceramic reinforcing phases with magnesium-based alloys might overcome this issue [9,10].

Parande et al. [11] examined eggshell powder reinforced with the Mg-Zn alloy and found that it improved its mechanical, damping, and grain refining capabilities significantly without significantly raising its density. Verma et. al. [12] investigated the Mg-Zn-Mn-Ca alloy, which was reinforced with ZnO. As a result, the ultimate and yield strengths in tension increased by 16% and 21%, and the ultimate compressive and compressive yield strengths increased by 23% and 26%, respectively. Jhamb et al. [13] examined the effect of Sn concentration on the Mg-Sn alloy. The study demonstrates that the rise in Sn concentration in the composite increases the mechanical behavior of the composite, but the corrosion resistance of the composite reduces with the rise in concentration. The 1 wt.% of Sn has better mechanical performance compared to the other 2 wt.% and 3 wt.% samples.

Zinc-reinforced pure Mg composites were studied by Chen et al. [14]. Their analysis revealed superior biodegradability, mechanical performance, and corrosion resistance due to grain refinement and intermetallic phases, which enhanced the quality of the composites. Zinc provided cathodic protection against corrosion and affected the biodegradation process of Mg. Improved behavior and biocompatibility make magnesium/zinc composites a promising option for orthopedic implantation. Wang et al. [15] reveal that the Mg/HA composite shows superior mechanical performance at a lower concentration of HA in the composite. This enhancement is due to the homogeneous distribution of the reinforced elements and the strong wetting that takes place between the matrix and the reinforcement. Liu et al. [16] demonstrated the incorporation of calcium phosphate into magnesium. Enhanced biocompatibility and mechanical performance include the hardness and compression strength of the composite as compared to pure magnesium. Zhang et al. [17] enhanced the compression and tribological behavior of the Mg composite with the inclusion of graphene particles. The incorporation of graphene led to a lower risk of infection in the implant region.

Hydroxyapatite (HAP) is an outstanding material for biomedical implantation because of its exceptional osteoconductivity and great biocompatibility, which promote the growth of bones as well as cooperation with the tissue surrounding it [18]. Naturally occurring bone can eventually replace the implant material due to its bioactive qualities. The incorporation of Zn and Sn into the biocomposite resulted in good antibacterial, biocompatibility, and mechanical performance in terms of strength, stiffness, and wear resistance [19,20].

There are surprisingly few studies examining all the mechanical behaviors of magnesium-based biocomposites containing hydroxyapatite, zinc, and tin, according to the additional literature survey [7–28]. Moreover, no research has been performed on the use of ultrasonic-assisted rheo-squeeze casting for producing magnesium-based biocomposites. This preliminary report systematically evaluated the influence of the fabrication technique and the effects of adding Zn and Sn on the mechanical performance of the composites. Consequently, the goal of this study is to close this gap by focusing on the fabrication and mechanical enhancement of Mg/HA, Mg/HA/Zn, and Mg/HA/Sn composites through the ultrasonic-assisted rheo-squeeze casting technique.

2. Materials and Method

In this study, pure magnesium ingots were purchased from a nearby supplier. The zinc (Zn), tin (Sn), and reinforcements in the form of 99% pure hydroxyapatite microparticles with a size of about 26 µm were purchased from MK Industries, Canada.

The pure Mg, Mg-5%HA, Mg-5%HA/1%Zn, and Mg-5%HA/1%Sn composites are made using a stir–squeeze casting setup that is connected to an ultrasonication facility [25]. Table 1 shows the weight percentage contribution of each item and the codes of the composites. The pure magnesium ingot of the calculated quantity is first held in a graphite crucible, heated to 720 °C inside a resistance furnace, and used to create the Mg-5%HA composite. To lessen the possibility of a rapid oxidation of magnesium, inert argon gas was passed at a rate of 4 mL/min. After that, HA particles were heated to 370 °C in an air oven before being introduced to the melt at 720 °C for ten minutes while being stirred continuously at 320 rpm with an impeller. Preheating the magnesium ingot and reinforcing particles prior to use inhibits the production of surplus gases during the melting process of the composite. This prevents cavities from forming during the casting process. In order to ensure that the clustered particles broke, the molten composite was further cooled to a semi-solid state at 520 °C. The melt was then heated to above the melting point of the magnesium (720 °C), and stirring was performed for 12 min at 320 rpm.

Table 1. Composite specimen codes and wt.% of elements.

Specimen Code	Magnesium (99% Pure)	Hydroxyapatite (mp) (99% Pure)	Zinc (99% Pure)	Tin (99% Pure)
Pure Mg	100%	-	-	-
MHA	95%	5%	-	-
MZHA	94%	5%	1%	-
MSHA	94%	5%	-	1%

Through this process, the reinforced particles are able to disperse evenly throughout the liquid melt. To further enhance the homogeneity of the particle distribution, the ultrasonication technique was employed. A titanium ultrasonic probe with dimensions of 22 mm in diameter and 210 mm in length was supplied by M/s. Johnson Plastosonic, Pune, India. The probe generated 22 kHz acoustic waves with 2.5 kW of power, a constant amplitude percentage, and an intensity of 42% and 42.61 W/cm^2. The ultrasonic probe was lowered approximately two-thirds of the way, and the melt was sonicated for 8 min. The impact produced by acoustic waves broke up the clusters of HA particles on the molten metal. The liquid combination was then placed over a 150 mm ×150 mm×50 mm steel die that had been warmed to 420 °C. After the composite melt was subjected to gravity and squeeze casting at 55 MPa for 10 min, the liquid solidified. The die was then left to come to room temperature. Preheating the steel die helps avoid localized stress concentrations that might lead to surface cracks. In order to conduct various tests, the solidified composites were eventually removed and were then ready for sample extraction. An analogous procedure was employed to fabricate all the composites.

3. Morphological and Mechanical Characterizations

The microstructural behavior of the composite was analyzed through Scanning electron microscopy (ZEISS SUPRA 55, Carl Zeiss AG, Oberkochen, Germany) with an acceleration voltage of 20 kV and a working distance of 10 mm, and a tungsten filament electron source was utilized. Additionally, elemental mapping of the fabricated composite was identified through FESEM (Carl Zeiss AG, Oberkochen, Germany). The phase analysis of the composites was performed through XRD X'pert Pro (Carl Zeiss AG, Oberkochen, Germany).

By using Archimedes' principle [24] (expressed in Equation (1)), the ASTM B962-13 [23] standard was adhered to in order to calculate the experimental density of the samples. The sample's porosity was computed, as Equation (2) illustrates. The ratio of mass-to-volume and Equation (1) were used to obtain the theoretical and actual densities, correspondingly.

$$\rho a = \text{dry wt.}/(\text{saturated wt.} - \text{suspended wt.}) \times \text{Water density value } (g/cm^3) \quad (1)$$

$$\text{Porosity} = 1 - [\rho_a - \rho_t] \quad (2)$$

where ρa = actual density, and ρt = theoretical density.

The microhardness of the composite was measured through the Vickers hardness tester (Krystal Elmec, Chennai, India) as per the ASTM E92 [23] standard. Material characterization for tensile, compression, flexural, (Tinious olsen H10KL, Horsham, PA, USA), and impact tests (Tinius Olsen—Imapct104, Horsham, PA, USA) was conducted following ASTM standards to ensure consistency and reliability of results. Three test repetitions were carried out for each specimen to ensure the consistency of the results.

Tensile tests were conducted in accordance with ASTM E8/E8M [23], which has a load-carrying capacity of 10 KN, with gauge lengths of 30 mm, thicknesses of 5 mm, and the cross head's speed is specified as 2.5 mm/min. Compression tests were conducted per ASTM E9 [23], and involved subjecting specimens to compressive forces to evaluate the properties with a load-carrying capacity of 10 KN. The specimen had a length of 19.2 mm and a diameter of 12.8 mm. Flexural tests, following ASTM D790 [23], measure the flexural modulus and strength of materials by applying bending loads to specimens. The specimen had dimensions of 125 × 12.7 × 6.4 mm and a span of 102 mm. Finally, impact tests, as per ASTM E23 [23], assess a material's toughness and resistance to fracture under dynamic loading conditions, typically using pendulum impact testers. The test specimen, measuring 55 × 10 × 10 mm with a V-notch in the center at an angle of 45° and 2 mm depth.

4. Results and Discussion

4.1. Morphology Behavior of the Composite Samples

Figure 1A–D illustrates the microstructural morphology of the pure Mg, MHA, MZHA, and MSHA composite samples. Figure 1A reveals the microstructure of pure Mg with visible cavities that arise due to the shrinkage effect during solidification. Figure 1B states that the MHA composite has demonstrated the distribution of included HA particles in the matrix, as indicated with yellow markers. Furthermore, some visible cavities and oxides (black patches) were also observed. Figure 1C demonstrates that the microstructure of the MZHA composite has shown agglomerated reinforced particles and a secondary MgZn phase. The intermetallic phases are identified through XRD analysis, as shown in Figure 2.

Figure 1D illustrates the microstructure of MSHA composites exhibiting well-bonded interfaces and an even distribution of reinforced HA particles in the magnesium matrix. Further, uniform distribution of secondary β-phases (Mg_2Sn) is also evident, as shown in Figure 2. From the overall observation, the utilization of the present composite fabrication technique resulted in the development of composites with proper distribution of the reinforcement phases with low casting defects. This could be attributed to the application of ultrasonic acoustic waves that had broken down the clusters of particles and helped them to distribute in the matrix phase. However, it is difficult to disclose the grain structure

of the casted samples, the grain refinement attainment was well established in previous research works and it was reported that grain size was reduced while adding Zn and Sn as alloying elements in the Mg matrix [18–20].

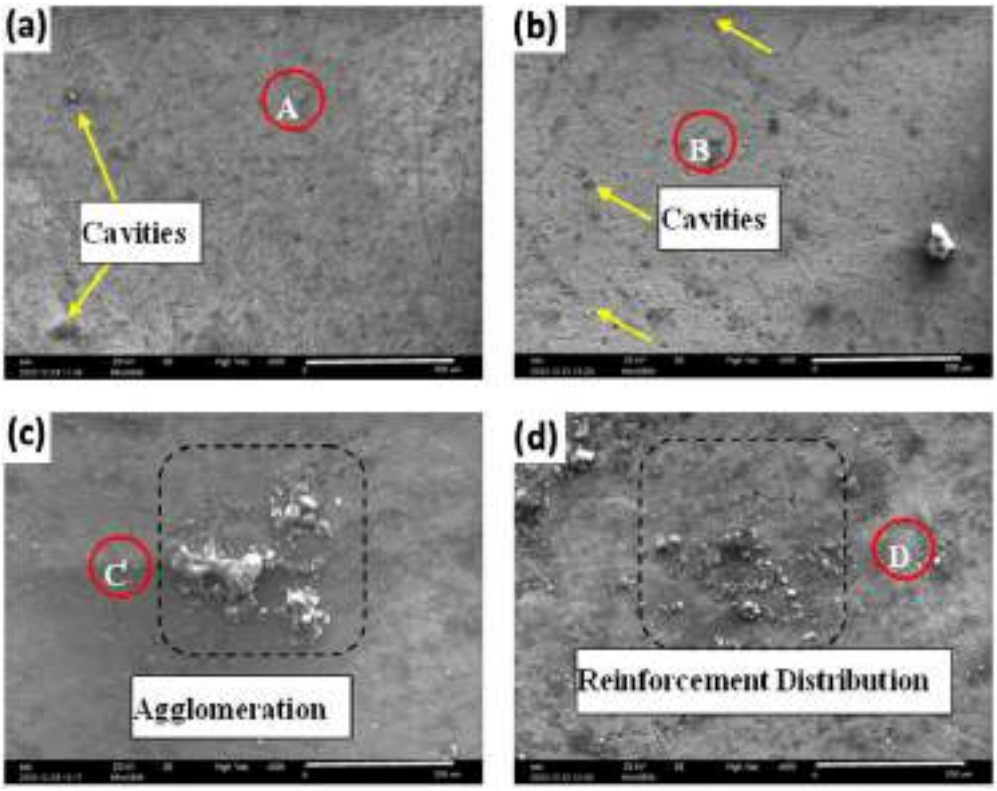

Figure 1. SEM microstructural view (**a**) pure Mg, (**b**) MHA, (**c**) MZHA, and (**d**) MSHA.

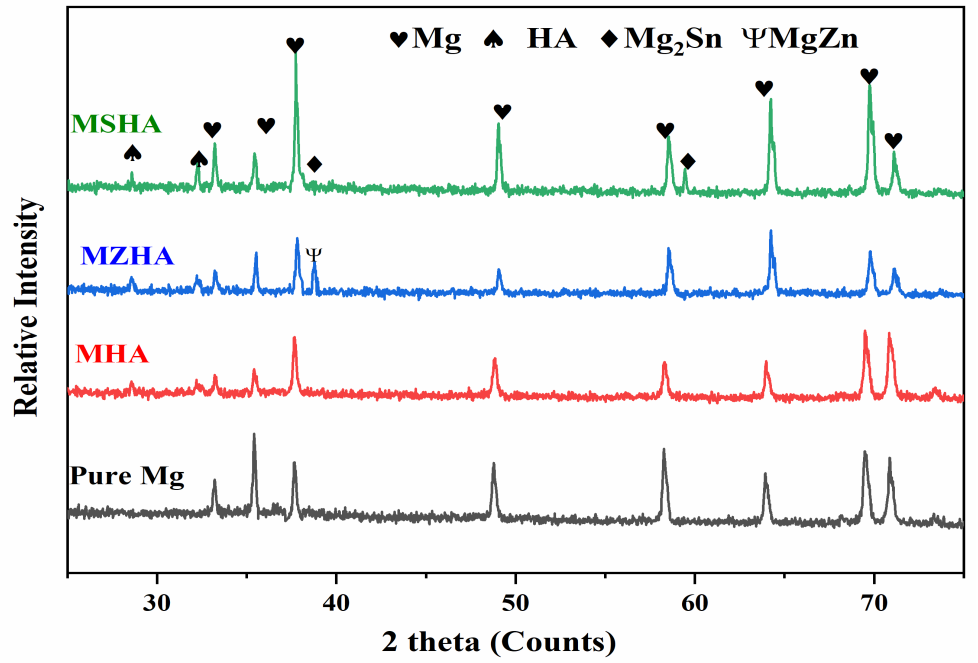

Figure 2. XRD analysis of the composites.

Figure 3 depicts the elemental mapping of the A-Pure Mg, B-MHA, C-MZHA, and D-MSHA composites, demonstrating the presence of Mg, O, Ca, and P elements in all the analyzed samples. This was taken from the locations A, B, C, and D encircled in Figure 1. The appearance of Ca and P are the constituent elements of bone which confirms the presence of hydroxyapatite. In the case of alloy matrix composites, along with the above elements, spectral peaks of Zn and Sn were also seen in the MZHA and MSHA composites, which evidenced the distribution of elements.

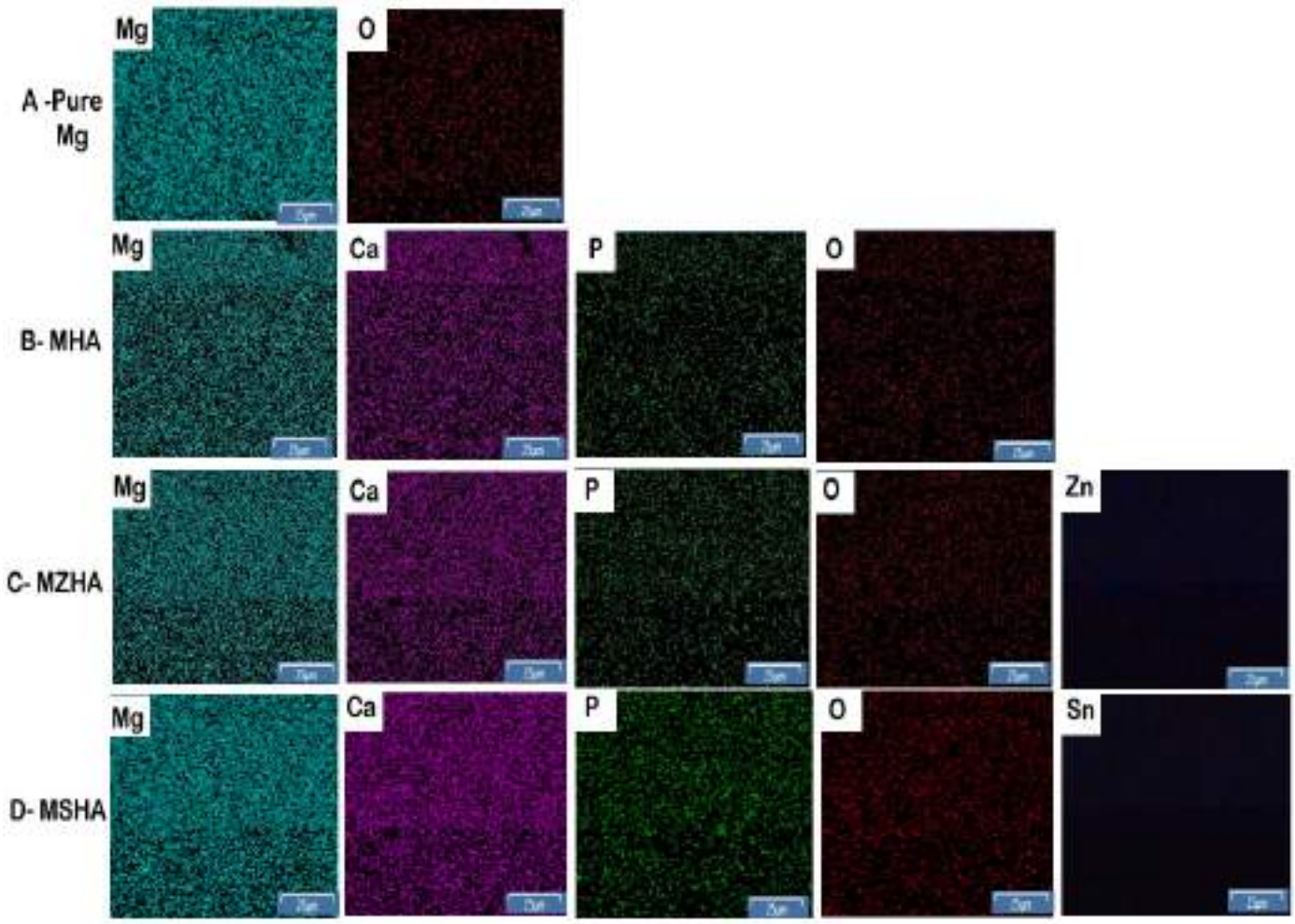

Figure 3. Elemental mapping of the (**A**) pure Mg, (**B**) MHA, (**C**) MZHA, and (**D**) MSHA.

4.2. Density and Porosity

The theoretical and actual densities of the fabricated composites, such as pure Mg, MHA, MZHA, and MSHA, exhibit significant disparities, as shown in Figure 4. Theoretical densities for pure Mg, MHA, MZHA, and MSHA stand at 1.73 g/cm^3, 1.79 g/cm^3, 1.81 g/cm^3, and 1.80 g/cm^3, respectively. However, through rheo-squeeze casting with ultrasonic assistance, actual densities are observed to be 1.73 g/cm^3, 1.71 g/cm^3, 1.79 g/cm^3, and 1.78 g/cm^3, respectively. These disparities can be attributed to particle agglomeration. Furthermore, pore formation and cavities were formed due to air bubbles that were entrapped during the stirring process, which also led to void formation. In spite of this, the composites show negligible void content with low porosity percentages of 0%, 0.05%, 0.04%, and 0.03%. The acoustic ultrasonic waves and applied squeeze pressure improve the distribution and enhance the proper wetting of reinforcements with the Mg matrix, resulting in good densification. However, porosity is common during the melting and solidification processes. It is worthwhile to note that the surface porosity of biomaterials can also be beneficial, especially when it comes to bone support fixtures, as the

pores might become active cell proliferation sites and promote cell adherence that may speed up the healing process of damaged bone tissues and aid in the osseointegration phenomenon [20].

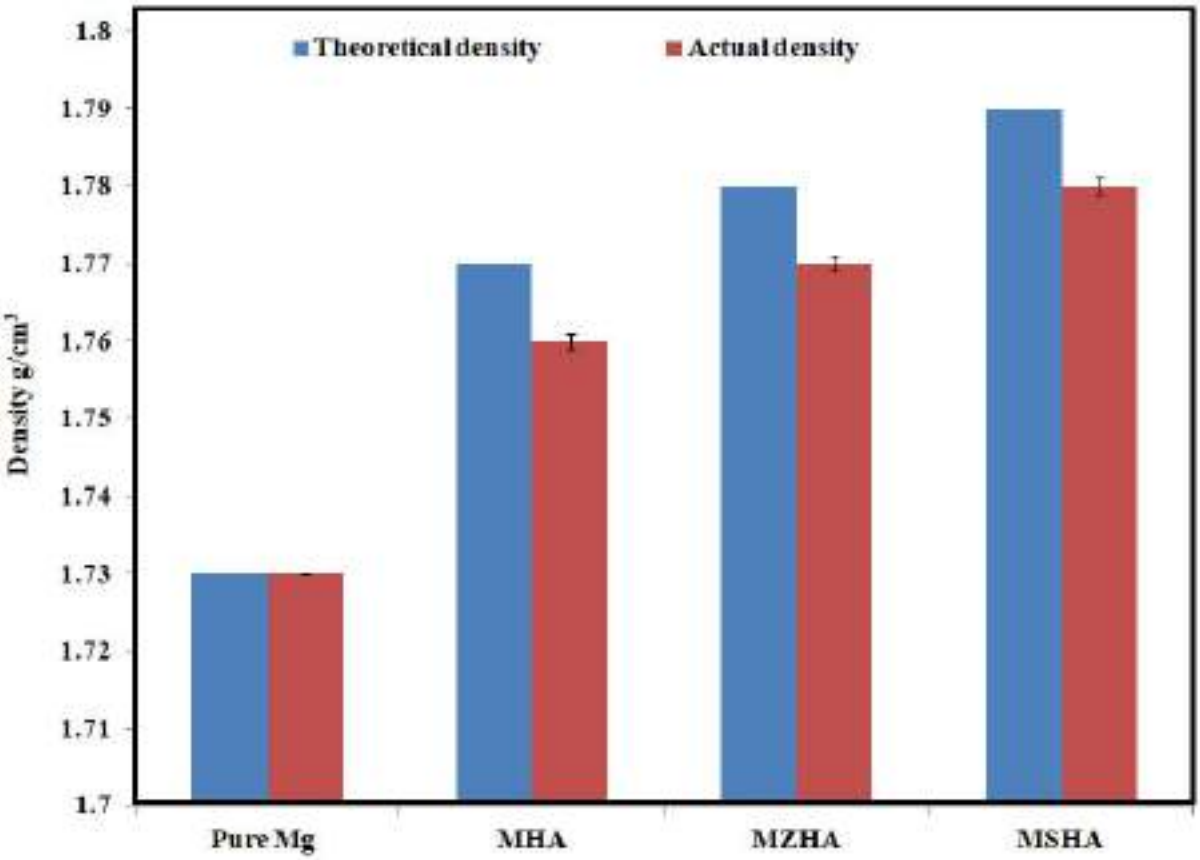

Figure 4. Theoretical and actual densities of pure Mg, MHA, MZHA, and MSHA.

4.3. Mechanical Properties

4.3.1. Microhardness

The microhardness test results of the squeeze rheocasted specimens indicate that the Zn and Sn alloy composites with HA reinforcements have significantly improved the hardness of the composites as shown in Figure 5. The MSHA composite outperformed all other tested materials, with a peak hardness of 95.1 HV, which is 64.5% more than that of unreinforced Mg. The improved hardness of the composites could be attributed to the inclusion of hard ceramic (HA) particles in the soft magnesium matrix. In particular, in the case of the MSHA composite, the distribution of HA and precipitated secondary Mg_2Sn phase impeded the local dislocation translation during indentation and opposed plastic deformation. Furthermore, the improved hardness in the MSHA composite could be further explained according to the Hall–Petch relation [28], which says that the strength of the material is inversely proportional to the grain size, i.e., the reduction in grain size improves the strength of the material. In this case, the refined grain structure of the MSHA composite could have effectively barricaded the dislocation movements during the localized impression of the indenter and resisted the deformation. This phenomenon is in good alignment with the previous research work reported by [19].

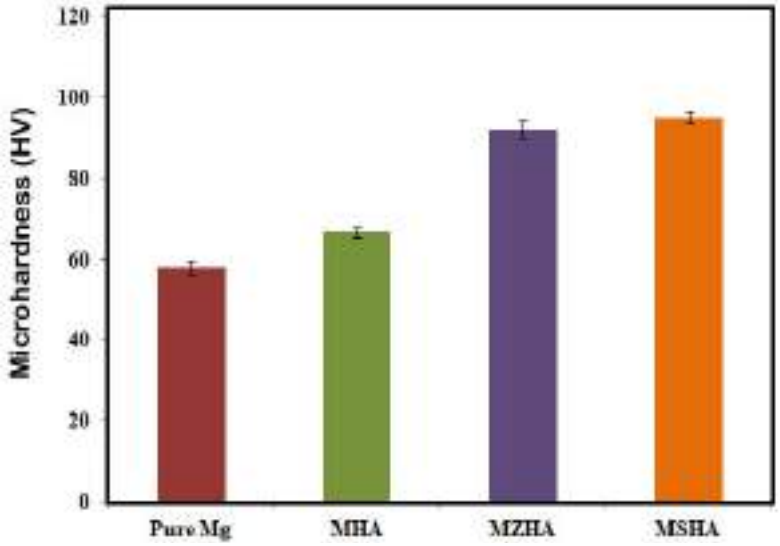

Figure 5. Microhardness behavior of the pure Mg, MHA, MZHA, and MSHA.

4.3.2. Compression and Tensile Performance of the Composites

Figure 6 illustrates the compressive and tensile behavior of the composite materials. It is noteworthy that the modest incorporation of Zn and Sn contributes to the improvement of mechanical characteristics in Mg composites. This enhancement is associated with grain refinement, facilitated by the presence of Sn and Zn, leading to the formation of robust intermetallic compounds, namely, Mg_2Sn and MgZn. The Mg_2Sn precipitates are uniformly dispersed throughout the matrix phase, whereas the dispersion of MgZn exhibits a lower rate and is clustered when compared to Mg_2Sn.

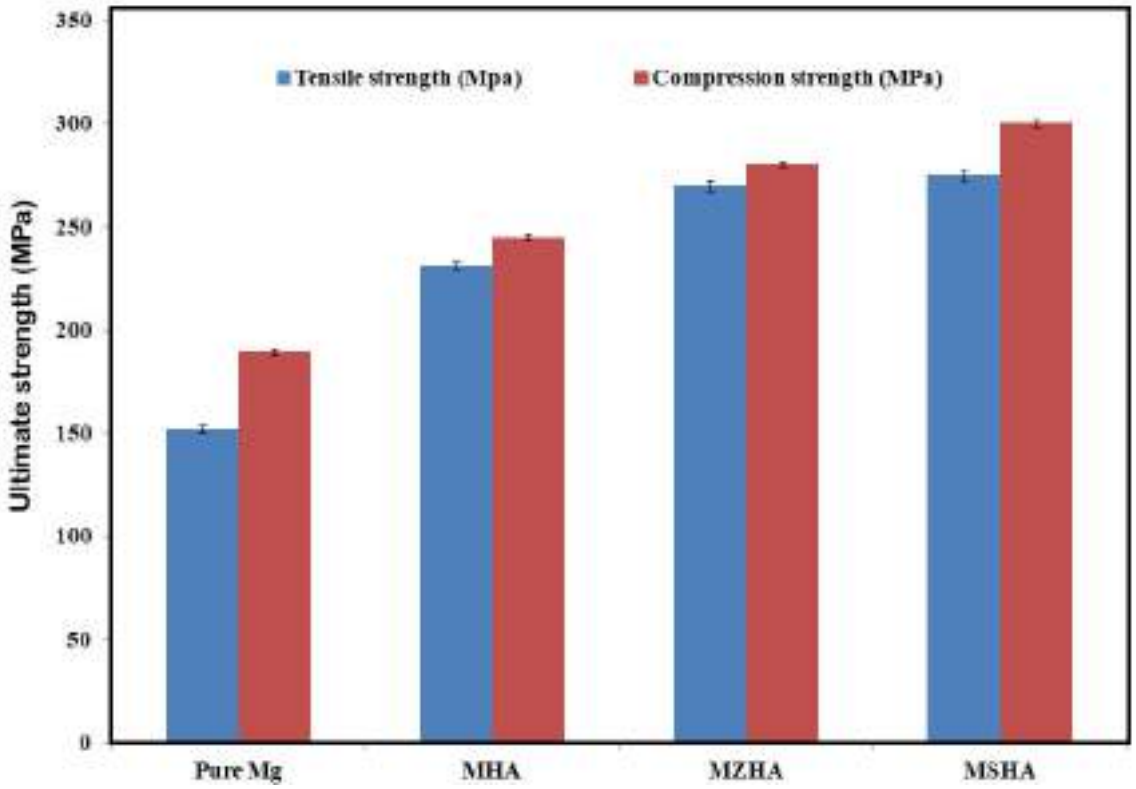

Figure 6. Tensile and compression strength of the pure Mg, MHA, MZHA, and MSHA.

The heightened strength demonstrated by Mg composites could be attributed to several strengthening mechanisms, as follows: (1) Dispersion strengthening: The dispersion of Sn within the matrix phase contributed to the dispersion strengthening, where the secondary phase of fine particles hinders dislocation movement. (2) Coefficient of Thermal expansion (CTE) between the matrix and reinforcement: the difference in CTE between the matrix phase and Sn alloying elements develop internal stresses upon cooling from processing temperature. (3) Orowan strengthening resulting in effective distribution of the load onto the robust reinforcement elements: the Orowan mechanism involves the interaction of dislocations with Sn alloying elements.

This interaction leads to improved mechanical properties as the load is effectively distributed throughout the composite, resulting in the enhanced mechanical performance of the composites and consequently diminishing the stress borne by the matrix.

The rigid HA particles act as barriers to impede dislocations within the grains, concurrently resisting deformative stress, thereby augmenting the compressive and tensile strength of the composite material. Furthermore, the good dispersion of HA particles in the α-Mg matrix has influenced the rise in both the compressive and tensile behavior of the composite by restricting its plastic flow and enveloping the eutectic phases [18].

Figure 7 depicts the stress–strain plots obtained from compressive tests. The yield strength of both MZHA and MSHA was found to be greater than that of MHA due to the presence of MgZn, Mg_2Sn, and HA particles, which enable the pinning operation that inhibits the twinning phenomena. Table 2 illustrates the compression test outcomes of the composites. The yield strength was tested at 0.2% strain offset for all specimens. The inclusion of HA, Sn, and Zn improved the modulus of elasticity of Mg, which serves to reduce the stress shielding ability. The range of this modulus of elasticity matches up to the value of natural bone [3].

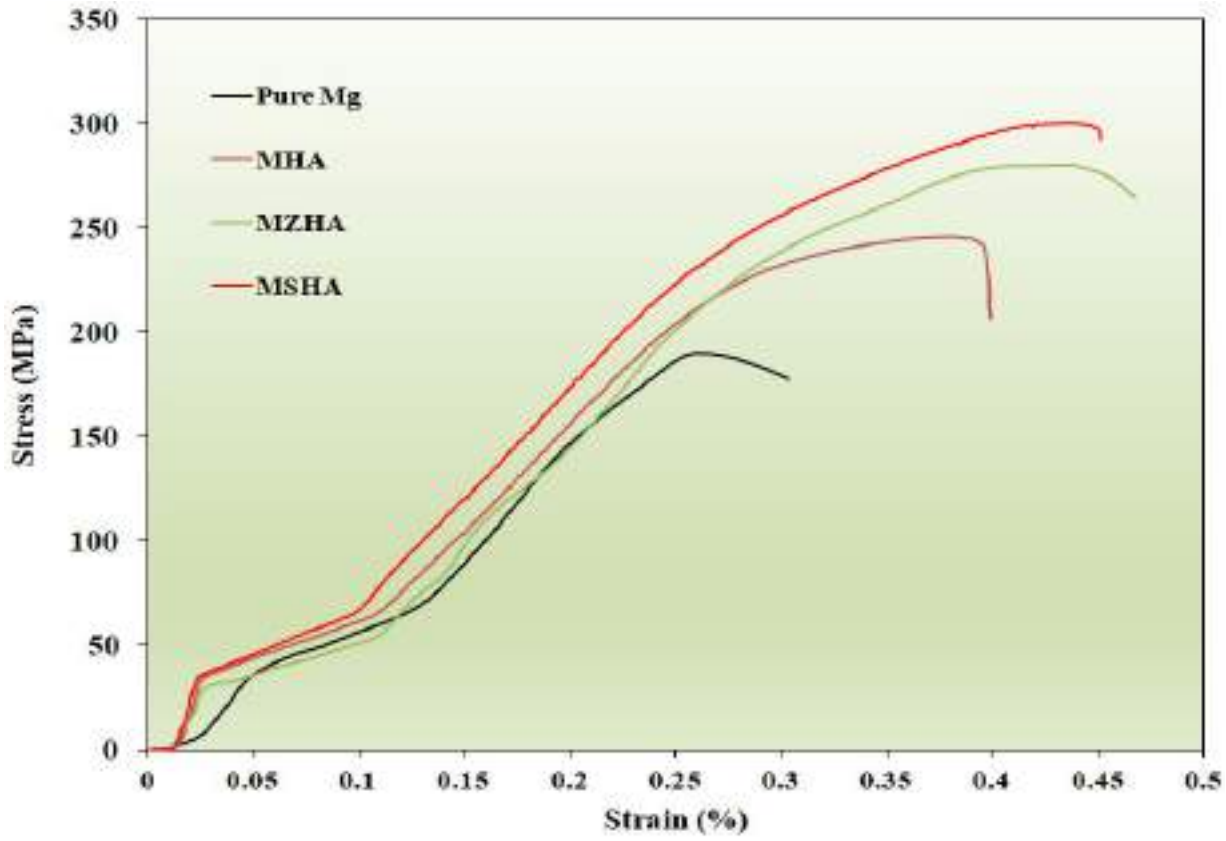

Figure 7. Stress vs. strain curve of the compression test of pure Mg, MHA, MZHA, and MSHA.

Table 2. Compression test outcomes of the composites.

Specimen Code	Yield Strength (Mpa)	Compression Strength (Mpa)
Pure Mg	110 ± 2	189 ± 1
MHA	130 ± 1	245 ± 3
MZHA	152 ± 3	280 ± 2
MSHA	180 ± 2	300 ± 2

When contrasting the MZHA outcome with that of MSHA, the MSHA composite yields superior results. This is due to the underlying chemical characteristics of Zn and Mg as well as the interfacial energy between them account for their reduced wettability. In particular, compared to the interaction between Mg and Sn, Zn and Mg do not establish as strong of a connection or spread across one other's surfaces because of their different atomic structures and surface energies. This may lead to less effective bonding and interfacial adhesion between the reinforcing phase and the magnesium matrix in composite constructions [8].

4.3.3. Impact and Flexural Behavior of the Composites

The impact and flexural strength of the composite materials are depicted in Figure 8. From the figure, it is evident that the MHA, MZHA, and MSHA have notably higher impact and flexural strengths compared to pure Mg. MSHA's impact and flexural properties are noticeably better than those of pure Mg, exhibiting improvements of 41% and 42%, respectively, and 8% and 7%, relative to MHA.

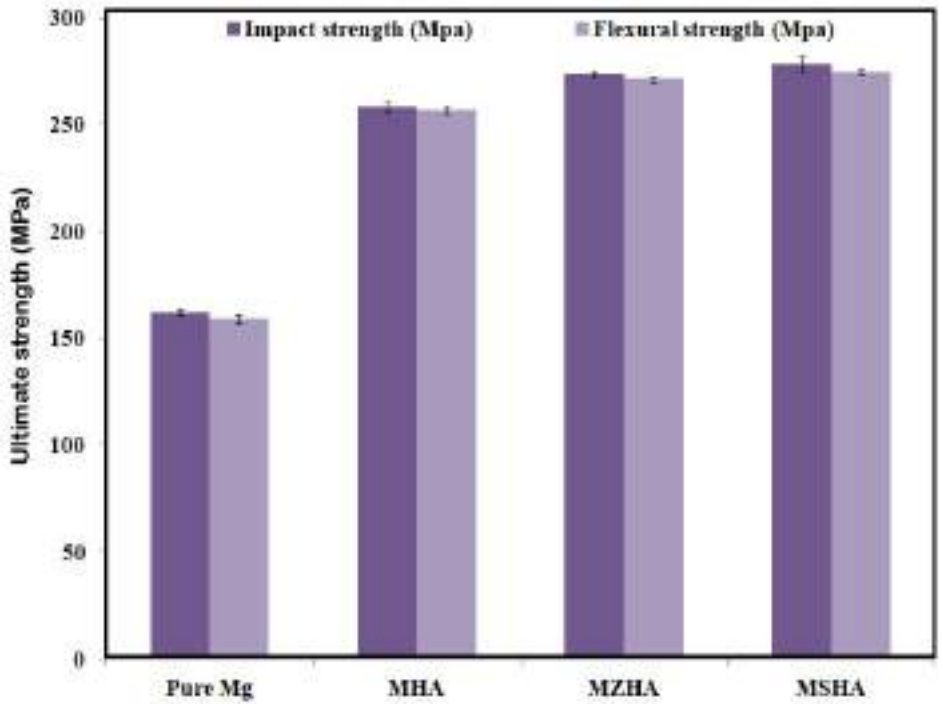

Figure 8. Impact and flexural strength of the pure Mg, MHA, MZHA, and MSHA.

By incorporation of the alloying element the intermetallic phases formed. The MZHA and MSHA composite are considerably strengthened by these intermetallic phases [7]. To enhance load transmission mechanisms and stop dislocation motions, these intermetallic phases are crucial. Grain size and grain boundary spacing are reduced when Zn and Sn aid in grain refinement within the Mg phase [18]. This grain refinement improves the impact and flexural performance of the composite by effectively inhibiting dislocation movement. The MZHA and MSHA composites' total strength and load transfer efficiency are increased by the better bonding. This is due to good interface bonding between the matrix and the alloying elements. Moreover, a uniform distribution of Zn and Sn

elements inside the matrix phase guarantees homogenous dispersion of strengthening agents [15], which contributes to the consistent mechanical performance of this composite. This synergistic rise results in improved strength, stiffness, and toughness for the composite material [23,25]. The MSHA composites showed enhanced impact and flexural behavior compared to the MZHA. Their decreased wettability can be attributed to the underlying chemical properties of zinc and magnesium, as well as the interfacial energy between them.

4.4. Fractographical Analysis of the Compression Tested Composites

The fractographical examination of the compressive samples, depicted in Figure 9a–d, reveals the presence of brittle and ductile fractures in the pure Mg, MHA, MZHA, and MSHA specimens. The fractured surface of the pure Mg, showcased in Figure 9a, shows a fracture pattern that is mostly ductile. Microscopic analysis of the broken surfaces revealed ductile deformation mechanisms, such as dimples, which are distinctive features. Yet, sporadic voids and micro-cracks were also noticed, indicating isolated regions of brittle fracture. Figure 9b displays a fractographical evaluation of the MHA, showing a blend of brittle and ductile fracture properties. The appearance of dimple-like deformation characteristics indicates that the addition of hydroxyapatite as a reinforcing material resulted in increased toughness. On the other hand, areas exhibiting micro cracks and voids suggested localized brittle fracture, potentially because of inadequate bonding between the reinforcement and matrix.

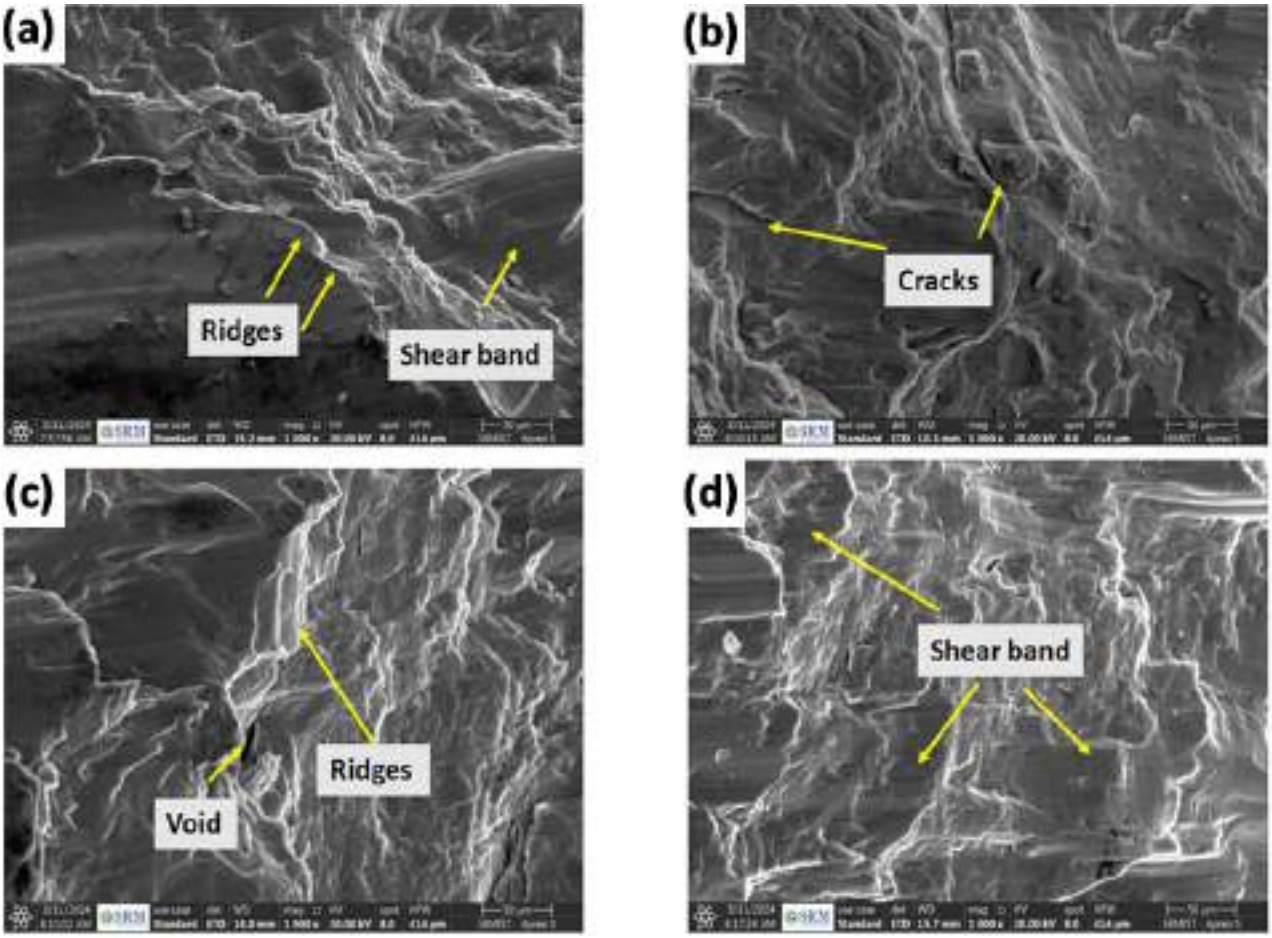

Figure 9. Fracture morphology of the compression test: (**a**) pure Mg, (**b**) MHA, (**c**) MZHA, and (**d**) MSHA.

As can be seen in Figure 9c, when compared to MHA, the MZHA composite showed better fracture resistance according to the compressive fractographical investigation. A decrease in micro cracks and voids was seen upon the inclusion of zinc as an extra reinforcement material, suggesting enhanced toughness and resistance to brittle fracture. Zn particle content appeared to effectively limit the propagation of cracks, which added to the overall performance of ductile fracture. Figure 9d illustrates that the MSHA composite showed significant improvements in toughness and fracture resistance after being subjected to compressive fractographical analysis. The use of tin as a reinforcing phase caused the distribution of reinforcement particles inside the matrix to become more consistent. Effective load and dissipation transfer occurred as a result, improving ductility and lowering the risk of brittle fracture. Few micro-cracks and voids were seen under a microscope, indicating a predominantly ductile fracture mechanism.

4.5. Effects of Zn and Sn in the Mg/HAP Composite

The influence of zinc and tin in Mg/HA composites fabricated using ultrasonic-assisted rheo-squeeze casting has played a vital role in tailoring the mechanical strength of the composites in terms of hardness, UTS, UCS, flexural, and impact behaviors. Both the alloying elements had the capability of improving the mechanical performance of the composite. Zinc increases material strength by distributing alloying elements within the matrix phase, and it enhances dispersion by inhibiting dislocation motion. Both zinc and tin inclusions show grain refinement during solidification and produce a microstructure with smaller, finer granules by separating at grain boundaries. However, Sn refined the grains comparatively less than Zn, which is evident due to the better hardness and mechanical properties of the MSHA [19,22]. Furthermore, Sn contributes to dispersion strengthening and shows uniform distribution of the secondary Mg_2Sn phase along the grain boundaries with good wettability with the soft Mg matrix. The secondary phases act as effective load-carrying catalysts and transfer the applied load from the matrix, impeding dislocation movement within the magnesium matrix thereby increasing the material's strength [19]. In summary, Mg-1%Sn/5% HA composites altered the strength of Mg/5%HA composites comparatively more than Zn and this makes them useful as potential materials for load-bearing bone fixture accessories to treat fractured bone.

5. Conclusions

Based on the experimental investigation outlined above, the following conclusions were drawn:

i. Pure Mg, MHA, MZHA, and MSHA were successfully manufactured through ultrasonic-assisted rheo-squeeze casting.
ii. From the microstructural observation, the inclusion of Sn elements in the matrix attains well-grained refinement and effectively stops dislocation movement compared to the MZHA, MHA, and pure Mg. This was evidenced by the improved mechanical characteristics.
iii. The MSHA composite demonstrates significantly superior mechanical performance compared to its MZHA, MHA, and pure Mg counterparts. Specifically, the microhardness of MSHA demonstrates a notable increase of 64.5% compared to pure Mg and 42.7% compared to MHA.
iv. In terms of tensile and compression behavior, MSHA exhibits remarkable enhancements of 80.8% and 58.3%, respectively, compared to pure Mg, and 19% and 22.4%, respectively, compared to MHA. Moreover, the impact and flexural properties of MSHA are notably improved, showing enhancements of 41% and 42% compared to pure Mg, and 8% and 7% compared to MHA, respectively.
v. The enhanced mechanical behavior of the MSHA composite could be attributed to the proper distribution of the Mg_2Sn phase that transfers load effectively from the matrix and prevents it from deforming.

Author Contributions: Conceptualization and project administration, A.T.; data curation, formal analysis, and writing—original draft, A.M.; visualization, R.P.R.B.; validation, W.W.F.C.; methodology, G.T.; supervision, M.G.; writing—review and editing, A.T., A.M., R.P.R.B., W.W.F.C., G.T. and M.G. All authors have read and agreed to the published version of the manuscript.

Funding: This work is partially funded by the Centre for Sustainable Materials and Surface Metamorphosis, Chennai Institute of Technology, India. Funding number: CIT/CSMSM/2024/RP/004.

Institutional Review Board Statement: Not applicable.

Informed Consent Statement: Not applicable.

Data Availability Statement: The original contributions presented in the study are included in the article, further inquiries can be directed to the corresponding authors.

Conflicts of Interest: Authors declare that there are no potential conflicts of interest.

References

1. Staiger, M.P.; Pietak, A.M.; Huadmai, J.; Dias, G. Magnesium and its alloys as orthopedic biomaterials: A review. *Biomaterials* **2006**, *27*, 1728–1734. [CrossRef] [PubMed]
2. Rosalbino, F.; De Negri, S.; Saccone, A.; Angelini, E.M.M.A.; Delfino, S. Bio-corrosion characterization of Mg–Zn–X (X= Ca, Mn, Si) alloys for biomedical applications. *J. Mater. Sci. Mater. Med.* **2010**, *21*, 1091–1098. [CrossRef] [PubMed]
3. Cui, Z.; Li, W.; Cheng, L.; Gong, D.; Cheng, W.; Wang, W. Effect of nano-HA content on the mechanical properties, degradation and biocompatible behavior of Mg-Zn/HA composite prepared by spark plasma sintering. *Mater. Charact.* **2019**, *151*, 620–631. [CrossRef]
4. Tayebi, M.; Bizari, D.; Hassanzade, Z. Investigation of mechanical properties and biocorrosion behavior of in situ and ex situ Mg composite for orthopedic implants. *Mater. Sci. Eng. C* **2020**, *113*, 110974. [CrossRef] [PubMed]
5. Barabás, R.; Fort, C.I.; Turdean, G.L.; Bizo, L. Influence of HAP on the morpho-structural properties and corrosion resistance of ZrO_2-based composites for biomedical applications. *Crystals* **2021**, *11*, 202. [CrossRef]
6. Avinashi, S.K.; Singh, P.; Sharma, K.; Hussain, A.; Singh, D.; Gautam, C. Morphological, mechanical, and biological evolution of pure hydroxyapatite and its composites with titanium carbide for biomedical applications. *Ceram. Int.* **2022**, *48*, 18475–18489. [CrossRef]
7. Papynov, E.K.; Shichalin, O.O.; Belov, A.A.; Buravlev, I.Y.; Mayorov, V.Y.; Fedorets, A.N.; Kornakova, Z.E. $CaSiO_3$-HAp Metal-Reinforced Biocomposite Ceramics for Bone Tissue Engineering. *J. Funct. Biomater.* **2023**, *14*, 259. [CrossRef] [PubMed]
8. Ahmadi, R.; Izanloo, S. Development of HAp/GO/Ag coating on 316 LVM implant for medical applications. *J. Mech. Behav. Biomed. Mater.* **2022**, *126*, 105075. [CrossRef] [PubMed]
9. Avinashi, S.K.; Shweta; Bohra, B.; Mishra, R.K.; Kumari, S.; Fatima, Z.; Gautam, C.R. Fabrication of Novel 3-D Nanocomposites of HAp–TiC–h-BN–ZrO_2: Enhanced Mechanical Performances and In Vivo Toxicity Study for Biomedical Applications. *ACS Biomater. Sci. Eng.* **2024**, *10*, 2116–2132. [CrossRef] [PubMed]
10. Verma, V.; Saha, J.; Gautam, A.; Pal, K. Investigation on microstructure, mechanical, biocorrosion and biocompatibility behavior of nano-sized TiO_2@ Al_2O_3 reinforced Mg-HAp composites. *J. Alloys Compd.* **2022**, *910*, 164866. [CrossRef]
11. Parande, G.; Manakari, V.; Kopparthy, S.D.S.; Gupta, M. A study on the effect of low-cost eggshell reinforcement on the immersion, damping and mechanical properties of magnesium–zinc alloy. *Compos. Part B Eng.* **2020**, *182*, 107650. [CrossRef]
12. Vignesh, P.; Ramanathan, S.; Ashokkumar, M.; Ananthi, V. Biodegradable Mg–3Zn alloy/titanium–hydroxyapatite hybrid composites: Corrosion and cytotoxicity evaluation for orthopedic implant applications. *Transactions of the Indian Institute of Metals* **2024**, *77*, 1701–1710. [CrossRef]
13. Jhamb, S.K.; Goyal, A.; Pandey, A.; Verma, M.N. Mechanical, wear, and degradation behavior of biodegradable Mg-x% Sn alloy fabricated through powder mixing techniques. *J. Mater. Eng. Perform.* **2023**, *32*, 7123–7133. [CrossRef]
14. Jiang, W.; Yu, W. In Vitro Degradation Behavior, Mechanical Properties, and Cytocompatibility of Biodegradable Mg-1Zn-xSn Alloys. *Crystals* **2022**, *12*, 1219. [CrossRef]
15. Zhao, W.; Wang, J.; Weiyang, J.; Qiao, B.; Wang, Y.; Li, Y.; Jiang, D. A novel biodegradable Mg-1Zn-0.5 Sn alloy: Mechanical properties, corrosion behavior, biocompatibility, and antibacterial activity. *J. Magnes. Alloys* **2020**, *8*, 374–386. [CrossRef]
16. Khalajabadi, S.Z.; Kadir, M.R.A.; Izman, S.; Ebrahimi-Kahrizsangi, R. Fabrication, bio-corrosion behavior and mechanical properties of a Mg/HA/MgO nanocomposite for biomedical applications. *Mater. Des.* **2015**, *88*, 1223–1233. [CrossRef]
17. Salleh, E.M.; Zuhailawati, H.; Mohd Noor, S.N.F.; Othman, N.K. In vitro Biodegradation and mechanical properties of Mg-Zn alloy and Mg-Zn-hydroxyapatite composite produced by mechanical alloying for potential application in bone repair. *Metall. Mater. Trans. A* **2018**, *49*, 5888–5903. [CrossRef]
18. Prakash, C.; Singh, S.; Farina, I.; Fraternali, F.; Feo, L. Physical-mechanical characterization of biodegradable Mg-3Si-HA composites. *PSU Res. Rev.* **2018**, *2*, 152–174. [CrossRef]
19. Radha, R.; Sreekanth, D. Mechanical, in vitro corrosion and bioactivity performance of Mg based composite for orthopedic implant applications: Influence of Sn and HA addition. *Biomed. Eng. Adv.* **2022**, *3*, 100033. [CrossRef]

20. Vignesh, P.; Ramanathan, S.; Ashokkumar, M.; Sonar, T.; Ananthi, V. Microstructure, Mechanical, and Electrochemical Corrosion Performance of Ti/HA (Hydroxyapatite) Particles Reinforced Mg-3Zn Squeeze Casted Composites. *Int. J. Met.* **2023**, *18*, 1348–1360. [CrossRef]
21. Hu, Y.; Guo, X.; Qiao, Y.; Wang, X.; Lin, Q. Preparation of medical Mg–Zn alloys and the effect of different zinc contents on the alloy. *J. Mater. Sci. Mater. Med.* **2022**, *33*, 9. [CrossRef] [PubMed]
22. Nazirah, R.; Zuhailawati, H.; Siti Nur Hazwani, M.R.; Abdullah, T.K.; Azzura, I.; Dhindaw, B.K. The Influence of Hydroxyapatite and Alumina Particles on the Mechanical Properties and Corrosion Behavior of Mg-Zn Hybrid Composites for Implants. *Materials* **2021**, *14*, 6246. [CrossRef] [PubMed]
23. Verma, V.; Singh, S.; Pal, K. Exploring the potential of Mg-Zn-Mn-Ca/ZnO composites as a biodegradable alternative for fracture fixation: Microstructural, mechanical, and in-vitro biocompatibility analysis. *Compos. Struct.* **2023**, *323*, 117431. [CrossRef]
24. Vignesh, P.; Ramanathan, S.; Ashokkumar, M. Evaluation of the wear performance of novel Titanium/hydroxyapatite-reinforced Mg–3Zn hybrid composites fabricated by squeeze casting. *J. Bio-Tribo-Corros.* **2023**, *9*, 38. [CrossRef]
25. Arunkumar, T.; Selvakumaran, T.; Subbiah, R.; Ramachandran, K.; Manickam, S. Development of high-performance aluminium 6061/SiC nanocomposites by ultrasonic aided rheo-squeeze casting method. *Ultrason. Sonochem.* **2021**, *76*, 105631. [CrossRef] [PubMed]
26. Prakash, C.; Singh, S.; Verma, K.; Sidhu, S.S.; Singh, S. Synthesis and characterization of Mg-Zn-Mn-HA composite by spark plasma sintering process for orthopedic applications. *Vacuum* **2018**, *155*, 578–584. [CrossRef]
27. Bakhsheshi-Rad, H.R.; Idris, M.H.; Abdul-Kadir, M.R.; Ourdjini, A.; Medraj, M.; Daroonparvar, M.; Hamzah, E. Mechanical and bio-corrosion properties of quaternary Mg–Ca–Mn–Zn alloys compared with binary Mg–Ca alloys. *Mater. Des.* **2014**, *53*, 283–292. [CrossRef]
28. Packkirisamy, V.; Sundaramurthy, R.; Mohankumar, A.; Sonar, T. Tribological and electrochemical corrosion behavior of binary Mg–3Zn novel hybrid composites for biodegradable implant applications. *Mater. Test.* **2024**, *66*, 675–686. [CrossRef]